Çanakkale Onsekiz Mart University

Journal of Advanced Research in Natural and Applied Sciences

dergipark.org.tr/tr/pub/jarnas

Open Access

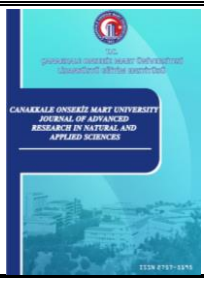

e-ISSN: 2757-5195 2024, Vol. 10, Issue 1, Pages: 21-32 doi.org/10.28979/jarnas.1318159

Corrosion Behaviors' Investigation of Carbide Coatings Developed for Sulphuric Acid Recovery Systems

Erhan Özkan[1]

[1]Dikkan R&D Center, İzmir, Türkiye

Article History

Received: 22 Jun 2023

Accepted: 28 Sep 2023

Published: 15 Mar 2024

Research Article

Abstract − In this study, corrosion resistance of cobalt and nickel, which are known to have high corrosion resistance, reinforced tungsten carbide coatings applied to low carbon stainless steel material surfaces to reduce corrosion-induced losses in sulphuric acid recovery systems were investigated. During the recovery of sulphuric acid, aggressive sulphur systems in the baths cause the metal surface to dissolve and therefore a high amount of material loss occurs. In order to minimize corrosion induced material loss, 316 L stainless steel surfaces were coated with an interlayer of 95% nickel and 5% aluminium alloy, and then tungsten carbide coatings were synthesized on the surfaces of substrate materials reinforced with 13% cobalt and 13% nickel, respectively by thermal spraying method to further reduce the corrosion rate. Characterization of the produced coatings were carried out by X-ray diffraction (XRD), scanning electron microscope (SEM), optical microscope, image analyzer, and surface roughness device. The standard potentiodynamic polarization characteristics of the coatings for 1M H_2SO_4 solution at room temperature were investigated with a potentiostat/galvanostat device. As the obtained results, nickel reinforced tungsten carbide coatings with nickel aluminium interlayer showed the highest corrosion resistance against sulfuric acid environment with 0,41 mm/year corrosion rate. As a result of the article, the corrosion resistance of 316L stainless steels in sulfuric acid systems was improved by 5.02 and 3.15 times, respectively.

Keywords − *Cobalt and nickel reinforcements, HVOF surface coating, stainless steel, sulphuric acid corrosion, tungsten carbide coatings*

1. Introduction

The most important problem encountered in sulfuric acid recovery plants is the presence of aggressive environments such as hydrogen sulfide and carbon dioxide, which cause corrosion damage to the materials [1]. Sulfuric acid (H_2SO_4) stands out as a chemical that is frequently found in structures in the petrochemical industry. The occurrence of sulfuric acid in the structures can be briefly summarized as follows: In converters, SO_2 from the raw material is oxidized to SO_3:

$$SO_2 + 1/2O_2 \rightarrow SO_3 \quad (1.1)$$

The gas in the reactors is exposed to high temperatures and as a result, it reacts with the water in the environment, causing the formation of sulfuric acid:

$$SO_3 + H_2O \rightarrow H_2SO_4 \quad (1.2)$$

Recycling facilities are of critical importance in terms of actively positioning sustainable ecosystem processes, which are one of the important issues of today, in the organization [2]. Sulfuric acid formed because of the above chemical reactions creates an aggressive corrosive environment in the main lines of petrochemical

[1]erhanozkan81@icloud.com (Corresponding Author)

industries and especially in sulfuric acid recovery plants [3]. Protecting metallic surfaces in recycling plants from corrosion, surface modifications of metals have come to the fore [4]. The corrosion resistance of materials can be increased by changing and improving the surface morphology and microstructure [5]. Changing the surface chemistry of materials; carburizing, nitriding, carbonitriding, boriding, siliconization and chroming processes are carried out [6]. In addition to all these, surface coating processes with thermal spraying have recently played a role in increasing the corrosion resistance of metallic surfaces to slow down the corrosion rate and make the surface corrosion resistance more effective [7].

Thermal spraying processes are carried out with spray guns to protect the main material surface from environmental conditions, to prevent corrosion, and to improve material surface properties [8]. After the coating material is melted with the energy used in the gun, it is thrown onto the material surface at high speed and the coating process is performed [9]. According to the type of energy supplied to the gun, there are two basic types of guns: guns that use electrical energy and guns that work with flame heating [10]. There are three types of gun systems that provide the energy required for melting fuel used flame like, flame spraying, spraying-fusing and HVOF (High Velocity Oxy-Fuel). Among these methods, especially the coatings produced with HVOF show very good adhesion and cohesion properties, as well as being very hard, making this method more advantageous than other methods [11]. Besides all these advantages, the formation of holes, pores, and micro-cracks because of high-temperature particles hitting the substrate surface at high speed can be counted among the disadvantages of this method [12]. These pores, cracks and holes have a negative effect on the corrosion behavior of the material [13]. In a corrosive environment, these structures act as channels between the coating and the substrate, causing the substrate material to be exposed to the corrosive environment [14]. This situation increases the diffusion of the corrosive environment and causes faster damage to the litter material [15]. To prevent this, systems have been developed by creating a buffer layer on the coatings [16]. Interlayers provide great advantages in preventing formations such as capillary cracks and porosity, which reduce corrosion resistance.

Due to its chemical content, 316 L quality stainless steels are widely used in systems that are expected to be resistant to aqueous corrosion, such as sea water and acidic solutions. It is defined as 1.4404 or X2CrNiMo17-12-2 according to EN, which is called European Norm Standards, and as S31603 according to UNS. The weakness of this product is that it cannot perform adequately in environments with more aggressive corrosion. For this reason, stainless steels called duplex stainless steel and defined as 1.4462 in the standard are widely used instead of 316 L stainless steel, but since the production of this type of steel is not common in our country, it is possible to obtain it from abroad. On the other hand, it is of critical importance for the sector to reduce the need for duplex quality stainless steels by improving the surface properties of 316 L quality stainless steel, which is widely produced in our country. In this study, the corrosion behavior of 316 L stainless steels, which are widely used in sulfuric acid recovery facilities in our country, with HVOF technique, and the surfaces coated with NiAl, WC-Co and WC-Ni in 1 M H_2SO_4 solution with standard potentiodynamic methods were investigated. Due to their high temperature resistance up to 1100 °C, NiAl coating was preferred as a buffer layer. Moreover, nickel-cobalt binary alloy coatings are widely used in qualified industries due to their properties such as high strength, corrosion, and wear resistance [17-19]. According to the results obtained, the records of increasing the service life of tungsten carbide coated stainless steels reinforced with different alloys in a corrosive environment were shared in detail. With these data, a roadmap has been presented regarding the basis of domestic and national solutions that will provide import substitution. In addition, information on the HVOF coating parameters, the porosity of the coating surfaces, the surface thicknesses and the corrosion behavior of the thicknesses and their interaction and changes were given in detail.

2. Materials and Methods

Experimental work steps consist of HVOF coating, characterization and analysis of coatings, corrosion tests, surface investigation and porosity determination. In Figure 1, there is a work-flow chart in which the experimental studies are symbolized as a single block.

Figure 1. Experimental work phases work-flow chart

2.1. HVOF Coating

316 L stainless steel samples with 50x50x2 mm dimensions were used as substrate material. Table 1 shows the mechanical properties of 316 L stainless steel, which is preferred as the substrate material.

Table 1. Mechanical properties of 316 L stainless steel material

Yield Strength (MPa)	Tensile Strength (MPa)	Hardness HRc
Min 170	Min 485	Max 22

Surface preparation of the samples to be used in the HVOF technique is an important step. This is because the adhesion of the coatings is directly related to the surface roughness and is controlled by the type of blast, pressure, angle, distance, time, and sandblast nozzle (hole size). Increasing the adhesion strength of the coating to the material surface, the material surface was sandblasted before proceeding to the HVOF thermal spray process. High hardness alumina particles were impinged on the material at high speed, increasing the roughness rate on the surface and increasing the number and size of asperities on the surface with increasing roughness. The particle coming to the surface during the spraying process clings to these asperities and attaches itself to this point mechanically and physically. High bond strength can only be achieved with the high roughness created. Therefore, the adhesion strength of the coating powders to the substrate surface increases. This was done with 35 grit alumina powders for 30 seconds using 400 kPa compressed air. HVOF process was carried out with Oerlikon Diamond Jet 2600 DJH brand system (Figure 2).

Figure 2. HVOF spray gun

Many carbide compositions, such as WC-based cermet carbides, have been successfully coated for the last 20 years using HVOF methods. Today these materials are used in the production of critical parts (piston and shaft, etc.) belonging to the aviation industry. HVOF coated WC-based cermet materials provide excellent toughness and high hardness. Moreover, WC-Co and WC-Ni cermet surface coatings are high hardness, wear resistance, widely used in many engineering parts as they have thermal stability and corrosion resistance. NiAl interlayer coatings were preferred because of their tribological properties. They have a critical role for the increasing

scratch resistance of the WC-based cermet carbides such as Co and Ni. Therefore, coating was obtained with conventional sintered powders with a grain size of 14 μm in the ratios of 13% by weight Co, 87% WC and 13% by weight Ni, 87%WC interlayer coating containing nickel and aluminium was carried out. The literature and previous studies were used to determine the content of the interlayer, and accordingly, NiAl powder containing 95% Ni and 5% Al by weight was used as the bond coating. The parameters of NiAl bond coating and WC-based two coatings are given in Table 2.

Table 2. Sputtering parameters of the HVOF process

Parameters	Values	
	NiAl	WC-based coatings
Oxygen flow (l min^{-1})	120	240
Fuel gas (hydrogen) flow (l min^{-1})	300	600
Carrier gas (nitrogen) flow (l min^{-1})	18	18
Spray distance (mm)	250	250
Substrate velocity (in the horizontal plane) (m s^{-1})	1	1
Gun velocity (in the vertical plane) (mm s^{-1})	5	5
Number of layers	20	20

2.2. Characterization and Analysis of Coatings

The characterization of the crystal structures of the coatings and the determination of the phases they contain were carried out with Rigaku D/Max-2200/PC model X-ray diffractometer, Cu-Kα (wavelength, λ=0.15418 nm) radiation.

The surface morphologies of the coatings, the structure and distribution of the particles, and their homogeneity at high magnifications were observed with a JEOL JJM 6060 scanning electron microscope (SEM). The coating thicknesses were measured with the LUCIA 4.21 image analyzer by placing the samples in a horizontal position.

Studies on the determination of the effect of surface roughness on adhesion and corrosion resistance and the comparison of post-corrosion surface roughness compared to the pre-corrosion situation were carried out with Mitutoyo SJ-301 device.

2.3. Corrosion Tests

Corrosion tests were carried out with GAMRY PC4/750 potentiostat/galvanostat. NiAl, WCCo/NiAl and WCNi/NiAl coated 316 L stainless steel samples were ultrasonically cleaned in acetone for 15 minutes before testing. Coatings with a surface area of 50x50 mm were placed in the corrosion cell by insulating only the coating surfaces in contact with the liquid. A 3-electrode system was used as a corrosion cell. Saturated calomel electrode (SCE) reference electrode, graphite rod auxiliary electrode and coated 316 L stainless steel samples were used as working electrodes. All experiments were carried out in 1 M H_2SO_4 solution and at temperatures between 24-27 °C. After the samples were placed in the solution, they were kept until they reached the open circuit potential (OCP). This value is defined as the value at which materials reach a constant potential. After this waiting, anodic polarization studies were carried out by applying potential to the coatings from below the open circuit potentials (approximately -500 mV) up to 4 V at a scanning rate of 5 mV s^{-1}.

The porosity of HVOF coatings was determined by electrochemical methods. The porosity of the coatings was calculated using the following equation [20].

$$F = \frac{R_{p,m}}{R_p} \log\left(\frac{-|\Delta E_{cor}|}{\beta a}\right) \tag{2.1}$$

The F in the equation gives the total porosity ratio in the coating. $R_{p,m}$ is the polarization resistance of the base material, R_p is the measured polarization resistance of the coating, ΔE_{cor} is the difference between the corrosion potentials of the base material and the coated material, and βa is the Anodic Tafel Slope of the base material.

After the corrosion tests, the corrosion rate was calculated in mm/year using the formula given below, using Faraday's Law, in order to meet the requirements of the ASTM G-102 standard.

$$CR = \frac{K \times W}{A \times T \times D} \tag{2.2}$$

3. Results and Discussion

3.1. Results

3.1.1. Phase Analysis and Microstructure

Figure 3 shows the XRD patterns of coatings synthesized with the NiAl interstage on stainless steel by the HVOF technique. The coatings' XRD patterns are defined as WC-Co/NiAl and WC-Ni/NiAl. WC-Ni/NiAl coatings included WC, W_2C, W, Ni, NiAl, Ni_3Al and FeNi phases. On the other hand, WC-Co, and WC, W_2C, W, Co, CoW_9C, $Co_8W_9C_4$, NiAl, Ni_3Al and FeNi phases were determined in the WC-Co/NiAl coatings. It has been observed that the WC, W_2C, W, C, Ni_3Al, FeNi phases were common in WC-Co/NiAl and WC-Ni/NiAl coatings. W_2C and metallic W phases obtained after deposition in both WC-based layers were formed by carbon loss during the coating process. Due to the NiAl bond layer on the substrate material, the presence of NiAl and Ni_3Al phases was observed in both samples. Islak and Buytoz [21] found similar findings in their study in 2013 and found that WC was the dominant phase in tungsten carbide reinforced coatings made with HVOF. As a result of decarburization during the spraying process, the WC phase was transformed into the W_2C phase. As the Ni addition amount increased, the intensities of the phases formed by W, C and Co elements decreased in a trace amount. Carbon, which is possible to form at high temperatures and liberated because of the decarburization of cobalt-containing phases, provided the formation of the triple $Co_8W_9C_5$ phase at very low rates [22].

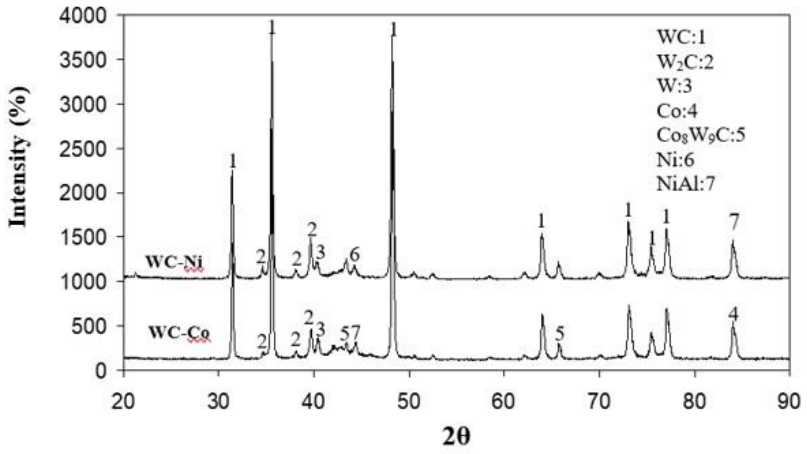

Figure 3. XRD patterns of samples coated with NiAl bond step on 316L stainless steel by HVOF technique a) WC-Co and b) WC-Nİ

A high percentage of pores, microcracks and unmelted particles were detected on the surfaces of WC-Co and WC-Ni coatings directly synthesized on 316L stainless steel without NiAl intermediate stage. The presence of these structures negatively affects corrosion, so SEM images of NiAl coated on stainless steel and WC-Co and WC-Ni coatings synthesized on this layer were evaluated and shown in Figure 4. Round particles were not observed in NiAl coatings, and this situation did not pose a great disadvantage because it is an intermediate layer, but it had a positive effect for better adhesion of the next layer. Due to the high melting temperature of the components in WC-Co coatings, the particles were synthesized in a smaller structure compared to WC-Ni coatings. The reason why the grain growth on WC-Ni coating surfaces is higher than on WC-Co coating surfaces is that the components in WC-Ni have relatively lower melting temperatures [23].

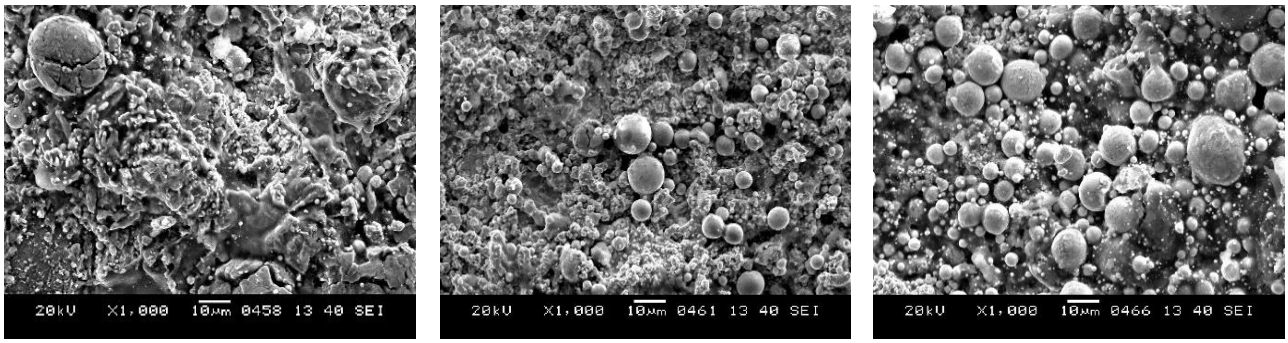

Figure 4. SEM images of coatings produced with HVOF (a) NiAl, (b) WC-Co, and (c) WC-Ni

3.1.2. Corrosion

In Figure 5, the time-dependent variation of corrosion potentials of NiAl bond coating, WC-Co and WC-Ni coatings on the main material 316 L, 316 L is given. The volt value, where the potential does not change over time, that is, the curve remains at a constant value, indicates the corrosion potential of the material (open circuit potential, equilibrium potential) [22]. By using the data in Figure 5, the equilibrium potentials of the samples were determined and scanning intervals were determined for the anodic polarization experiments, but 316 L stainless steel samples gave a more stable curve due to their bright and homogeneous surfaces. Since the NiAl bond coating surfaces are not homogeneous and have a rougher structure, it has shown a continuously decreasing curve characteristic. In Figure 4a, the absence of particle morphology in the NiAl microstructure and the heterogeneous microstructure on the surface and the inability of the curve to reach a constant potential overlap [24]. WC-Co and WC-Ni coatings, on the other hand, have a more homogeneous surface compared to NiAl and a more heterogeneous surface compared to 316 L, but when compared to each other, close curves are expected and a positive result. As a result of the comparison of the microstructures in Figure 4b and Figure 4c, the dense structure of the spherical particles on the surface confirms this data. Since an evaluation made according to the data in Figure 5 gives a misleading result, another evaluation method was preferred according to the anodic polarization curves. This situation gave similar results to literature 23studies. The main reason for this is that the corrosion potential is a calculated potential to find the Thevenin Equivalent Voltage between any two points. Considering the distance between two points as if it is an open electrical circuit, the potential difference between those two points is determined by using the voltage values at the other ends. For this reason, the more homogeneous and smooth the system surface, the healthier and cleaner the curves will be [12].

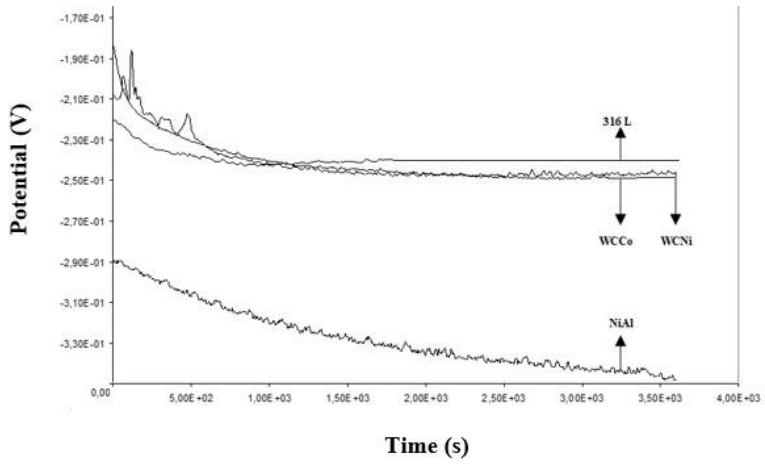

Figure 5. Time-dependent variation of corrosion potentials of substrate (316 L) and coatings (NiAl, WCCo, WCNi)

In Figure 6, the anodic polarization curves of the 316 L stainless steel sample, which is the base material, and the NiAl, WC-Co and WC-Ni coatings synthesized on it are given. The values of corrosion current (I_{cor}), corrosion potential (E_c), polarization resistance (R) and Tafel coefficients related to potentiodynamic polarization parameters are given in Table 3. Considering the Tafel curves (Figure 6) obtained in a 1 M H_2SO_4 corrosion environment, the corrosion resistance of WC-Co and WC-Ni based coating layers in the relevant corrosive environment is relatively higher compared to the substrate material, corrosion current and corrosion potential. values (Table 3). On the other hand, it was determined that the polarization resistance values were higher on the WC coated surfaces compared to the uncoated and only NiAl coated surfaces. There is a net current at the corrosion potential, but this current is not read because the total anodic current is equal to the total cathodic current. Corrosion current value is determined with this current, which is not directly measured. The current density obtained by dividing the corrosion current by the surface area of the electrode gives the corrosion rate of the metal. Since sulfuric acid affects both anodic and cathodic reactions with tungsten carbide, no great change in corrosion potentials was observed, but the corrosion current density decreased, and the polarization resistance increased. The effectiveness of HVOF coatings, calculated according to the corrosion current density and polarization resistance, increased as the corrosion resistance of the reinforcement material increased. The fact that the tungsten carbide efficiency obtained according to the polarization resistance and current density is similar, shows that there is a parallelism in the decrease of current and increase in resistance [11].

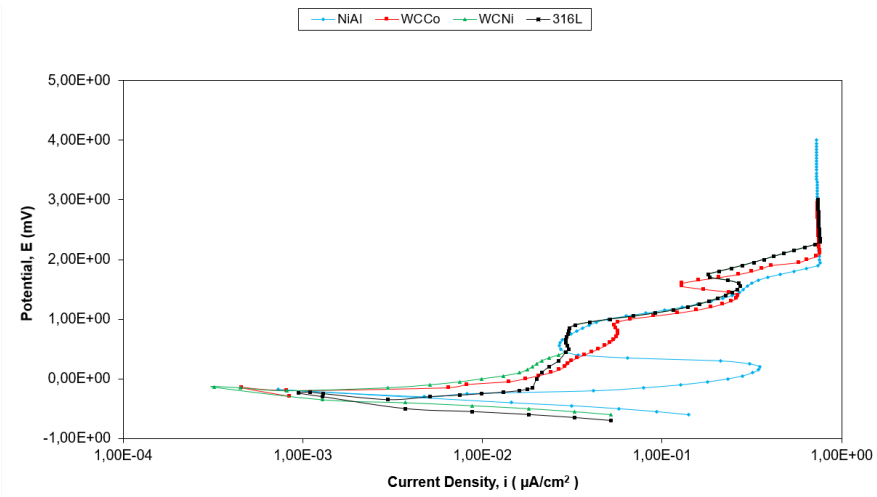

Figure 6. Anodic polarization curves of the samples

The slope values have been taken from the anodic and cathodic Tafel Polarization Curves, and it has been observed that there was correlation between the porosity values. Corrosion current was measured lower by coating 316L stainless steels. In all the results obtained, βa was greater than βc. This is an indication that oxide films protect the base material anodically [25]. The corrosion rate decreased by coating the surfaces with tungsten carbide. According to the results from Table 3, WC-Ni is the coating with the highest corrosion resistance, while the WC-Co coated material has a corrosion resistance close to WC-Ni. NiAl coating, on the other hand, has a lower corrosion resistance than WC-Ni and WC-Co but better than 316 L. The relationship between the advancement mechanism of the resulting structure and porosity has been established. It has been observed that WC-Ni and WC-Co coatings corroded in proportion to porosity, but NiAl interlayer coatings had the lowest corrosion resistance. Explaining this situation, porosity distribution should also be taken into consideration. Porosities that were small and homogeneously distributed throughout the coating structure cannot prevent the crystals formed because of the corrosion from progressing. Large porosities cannot prevent the crystals formed regarding to the corrosion. However, local porosities formation in crystals have been observed. This condition has a role in hindering progress [24].

Table 3. Electrochemical measurements of coatings in 1M H_2SO_4 solution at 25 ºC

Sample	E_c (mV)	β_c (mV)	β_a (mV)	I_{cor} (A)	Pol.Res. (R) (Ω)	Porosity (%)
316L	-240	31,87	256,6	94,6 x 10^{-5}	4,83 x 10^6	-
NiAl	-180	309,4	312,3	72,7 x 10^{-5}	3,90 x 10^6	8,24
WC-Co	-150	283,9	375,0	45,9 x 10^{-5}	2,66 x 10^6	6,58
WC-Ni	-140	31,87	256,6	32,2 x 10^{-5}	1,83 x 10^6	7,61

In order to compare the corrosion resistance of WC-Ni and WC-Co coatings more concretely, porosity values were considered. When the porosity amounts calculated by electrochemical methods were compared, it was observed that WC-Ni with larger nucleation had a higher porosity than WC-Co and this observation was confirmed by SEM pictures, but this research made from a small surface does not reveal a very accurate comparison criterion [23]. For this reason, the corrosion rates of WC-Ni and WC-Co coatings calculated with ASTM G-102 Faraday's Law are given in Table 4.

Table 4. Corrosion rate values of NiAl, WC-Ni, and WC-Co coatings

Sample	Corrosion Density (μA/cm^2)	Corrosion Rate (mm/year)
NiAl	22,72	2,05
WC-Co	14,30	1,29
WC-Ni	11,90	0,41

WC-Ni coating, calculated by Faraday's Law, has a lower corrosion rate of 14,6% compared to WC-Co. In other words, WC-Ni coated 316 L material will lose 0,88 mm less material due to corrosion in 1 M concentration H_2SO_4 solution in 1 year compared to WC-Co coated material. Determining the corrosion rate, which is defined as the amount of metal dissolving per unit time, is important for determining the corrosion resistance of metals and their alloys. Corrosion rate is measured quantitatively by mass loss, Tafel extrapolation method, linear polarization method and alternating current impedance measurement. Homogeneous mass loss measurement is one of the most accurate methods that will give a healthy and accurate result in determining the corrosion rate [25]. Although the reliability of Table 4 data is higher, its overlap with Table 3 data indicates a healthy comparison.

In Figure 7, SEM images taken after the corrosion test of the coatings are given. According to these images, it is clearly seen that the morphology of the coating has changed and especially the particle structure has deteriorated after the corrosion test. Along with the increase in the amount of Co in the WC-Co alloy coating electrolyte, an increase in the amount of Co% in the coating layer was observed. A decrease of % Co of WC-

Co alloy was determined with the increase of % Co. The mass fraction of cobalt in the coating is always greater than the concentration of Co^{+2} ions in the electrolyte. This is related to the unusual behavior of the WC-Co alloy coating, which is consistent with the results of previous researchers, and explains the reason for the particles remaining spherical after corrosion in Figure 7b [24].

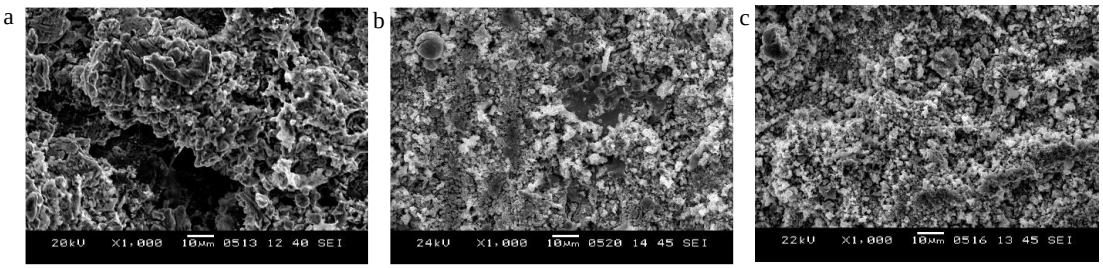

Figure 7. SEM images of coatings after corrosion test (a) NiAl, (b) WC-Co, and (c) WC-Ni

From the images in Figure 7, it cannot be concluded which coating alone suffers more material loss due to corrosion. From the SEM images, only the deformation occurring in the morphology before and after corrosion is detected, microstructure change, and thickness measurement should be made from the section to see the corrosion effect [15]. In order to reach this conclusion, the images given in Figure 8 provide a more accurate comparison.

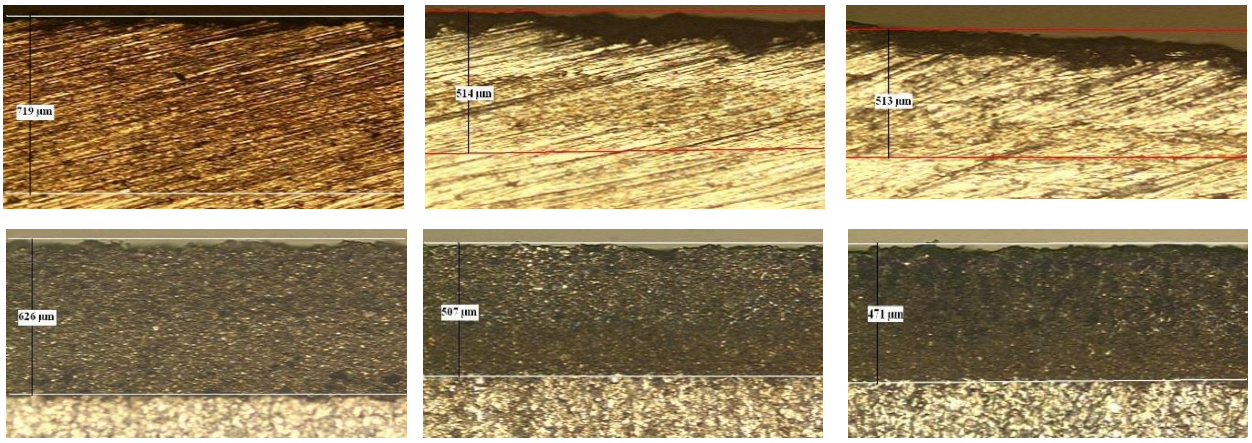

Figure 8. The view of the pre-corrosion and post-corrosion sections of the coatings and the measurement of the coating thickness (a) NiAl (P.C.) (b) NiAl (A.C.) (c) WCNi (P.C.) (d) WCNi (A.C.) (e) WCCo (P.C.) and (f) WCCo (A.C.) *(P.C.: Pre-Corrosion, A.C: Post-Corrosion)

Since the stoichiometric weights of the compared materials are close to each other, a relationship to be established between the weight loss and the amount of wear on the surface will not be very misleading [13]. The results of the thickness change in Table 5 and the corrosion rate and mass loss data exactly match. Accordingly, the most corrosion resistant nickel-reinforced tungsten carbide coating was determined.

Table 5. Changes in coating thickness

Sample	Pre-Corrosion	Post-Corrosion	Change in Thickness (%)
NiAl	719 µm	626 µm	12,93
WCNi	514 µm	507 µm	1,36
WCCo	513 µm	471 µm	8,19

3.2. Discussion

Phase analysis, microstructure control and electrochemical corrosion properties of WC-Ni/NiAl and WC-Co/NiAl samples coated with HVOF were investigated to improve the corrosion resistance and increase the

service life of 316 L stainless steel materials, which are widely used in sulfuric acid recovery plants, and the following results were obtained:

- WC-Co and WC-Ni coatings applied directly on 316 L material with the HVOF method were not coated alone due to their negative surface properties but were coated with NiAl interlayer to obtain positive surface properties.

- According to XRD results, W_2C and metallic W phases obtained after deposition in both WC-based layers were formed by carbon loss during the coating process.

- It was observed that NiAl and Ni_3Al phases were common in both samples due to the NiAl bond layer on the substrate.

- The corrosion potentials of NiAl, WC-Co/NiAl, WC-Ni/NiAl coatings and 316 L stainless steel were measured as -180, -150, -140 and -240 mV, respectively. Among the coatings, WC-Ni/NiAl was found to have the highest corrosion resistance against the sulfuric acid environment.

- The porosity ratios of the coatings were determined as 8,24% for NiAl, 6,58% for WC-Co and 7,61% for WC-Ni in the measurements made by electrochemical methods, but this calculation method is a method that can be widely used because it includes a small area. It cannot be preferred; it only gives an idea among the materials to be compared.

- The increase in the surface roughness caused a decrease in the polarization resistance of the samples.

- While the pre-corrosion thicknesses of NiAl, WC-Ni, WC-Co coatings were 719, 514 and 513 μm, respectively, these values were measured as 626, 507 and 471 μm after corrosion.

4. Conclusion

As a result, tungsten carbide-based, nickel and cobalt reinforced coatings have been successfully synthesized on 316 L stainless steel surfaces by HVOF method. The tungsten carbide phase naturally predominates in the XRD patterns. In SEM photographs, it was determined that the coatings covered the entire substrate homogeneously and were effective in anodic protection. The corrosion potentials of NiAl, WC-Co/NiAl, WC-Ni/NiAl coatings and 316 L stainless steel were measured as -180, -150, -140 and -240 mv, respectively. Among the coatings, WC-Ni/NiAl was found to have the highest corrosion resistance against sulfuric acid environment. As a result of detailed investigations of corrosion behavior, nickel-reinforced tungsten carbide coatings gave the best corrosion resistance with 0,41 mm/year corrosion rate. Due to the preference of HVOF technique, in which the parameters can be kept under stable control, certain increase or decrease in the measured values have been observed [15]. In addition, applying coatings to well-polished 316L stainless steel surfaces was another application example that supports this issue [22]. In our country, where recycling facilities have gained importance, studies are continuing to improve the material properties used in sulfuric acid recycling systems. As a result of this article, prepared for the purpose of improving the sulfuric acid corrosion resistance of 316 L quality stainless steels, an effective solution will be provided with completely national and domestic investments.

Author Contributions

The author read and approved the final version of the paper.

Conflicts of Interest

All the authors declare no conflict of interest.

References

[1] U. Yurt, B. Dündar, E. Çınar, *Jeopolimer betonlarda sülfürik asit etkisinin araştırılması,* Düzce Üniversitesi Bilim ve Teknoloji Dergisi 8 (2) (2020) 1548–1561.

[2] Ö. Tezel, S. Küçükkancabaş, E. Yıldız, *Sürdürülebilir kalkınma hedefleri bakımından atık yönetimi uygulamalarının hanehalkı tarafından değerlendirilmesi: Edirne örneği*, Trakya Üniversitesi Sosyal Bilimler Dergisi 22 (2) (2020) 941–957.

[3] İ. Dehri, M. Özcan, H. Sözüsağlam, (2000). *Polyester kaplamalı galvanize çelik üzerine SO_2 ve NH_3 gazlarının korozif etkilerinin EIS yöntemi ile belirlenmesi*, VII. Uluslar Arası Korozyon Sempozyumu, İstanbul, 2000, p. 246.

[4] Z. Ahmad, Principles of Corrosion Engineering and Corrosion Control, Butterworth-Heinemann, Oxford, 2006.

[5] P. R. Roberge, Corrosion basics: An introduction, 3rd Edition, National Association of Corrosion Engineers, Houston, 1984.

[6] J. Stokes, The Theory and Application of the HVOF Thermal Spray Process, Dublin City University, Dublin, 2005.

[7] H. Çuğ H, M. E. E. Erhaima, *Effect of Mn and Zr addition on microstructure, wear and corrosion behavior of Ti-6Al-4V composite biomaterials produced by powder metallurgy*, Manufacturing Technologies and Applications 2 (2) (2021) 41–48.

[8] H. V. Özkavak, Ş. Ş. Özcan, *yüksek hızlı oksi-yakıt (HVOF) yöntemiyle kaplanmış çelik ve alüminyum alaşımlarının aşınma özelliklerinin taguchi metoduyla optimizasyonu*, BEÜ Fen Bilimleri Dergisi 9 (2) (2020) 931–942.

[9] G. Koga, R. Schulz, S. Savoie, A. Nascimento, Y. Drolet, C. Bolfarini, C. Kiminami, W. Botta, *Microstructure and wear behavior of Fe-based amorphous HVOF coatings produced from commercial precursors*, Surface and Coatings Technology 309 (2017) 938–944.

[10] A. K. Lakshminarayanan, V. E. Annamalai, K. Elangovan, *Identification of optimum friction stir spot welding process parameters controlling the properties of low carbon automotive steel joints*, Jmaterrestechnol 4 (3) (2015) 262–272.

[11] G. Singh, N. Bala, V. Chawla, *High temperature oxidation behaviour of HVOF thermally sprayed NiCrAlY coating on T-91 boiler tube steel*, Materialstoday: Proceedings, 4 (4) (2017) 5259–5265.

[12] T. S. Sidhu, S. Prakash, R.D. Agrawal, *State of the Art of HVOF Coating Investigations–A Review*, Marine Technology Society Journal, 39 (2) (2017) 53–64.

[13] N. Singh, G. Vinay, D. Mahajan, *Cavitation erosion mechanisms of HVOF–sprayed Ni–based cermet coatings in 3.5% NaCl environment*, Surface and Coatings Technology, 434 (9) (2022) 128194.

[14] S. Candan, *An investigation on corrosion behaviour of pressure infiltrated Al–Mg alloy/SiCp composites*, Corrosion Science 51 (6) (2009) 1392–1398.

[15] H. M. Zakaria, *Microstructural and corrosion behavior of Al/SiC metal matrix composites*, Ain Shams Engineering Journal, 5 (3) (2014) 831–838.

[16] Y. H. Yoo, D. P. Le, J. G. Kim, S. K. Kim, P. V. Vinh, *Corrosion behavior of TiN, TiAlN, TiAlSiN thin films deposited on tool steel in the 3.5 wt.% NaCl solution*, Thin Solid Films 516 (11) (2008) 3544–3548.

[17] M. Ishikawa, H. Enomoto, M. Matsuoka, C. Iwakura, *Effect of tetraborate ions on electrodeposition of nickel-copper alloy from a pyrophosphate bath*, Electrochimica Acta 39 (14) (1994) 2153–2157.

[18] G. Qiao, T. Jing, N. Wang, Y. Gao, X. Zhao, J. Zhou, W. Wang, *Effect of current density on microstructure and properties of bulk nanocrystalline Ni–Co alloys prepared by JED*, Journal of The Electrochemical Society, 153 (5) (2006) C305–C308.

[19] C. U. Atuanya, D. I. Ekweghiariri, *Experimental correlation between varying processing properties and wear behaviour of ternary Ni-Co-SiO2 composites coating of mild steel*, The International Journal of Advanced Manufacturing Technology, 88 (9–12) (2017) 2581–2588.

[20] B. C. Oberländer, E. Lugscheider, *Comparison of properties of coatings produced by laser cladding and conventional methods*, Materials Science and Technology 8 (8) (1992) 657–665.

[21] S. Islak, S. Buytoz, *Microstructure properties of HVOF-sprayed NiCrBSi/WCCo-based composite coatings on AISI 1040 steel*, Optoelectronics and Advanced Materials–Rapid Communications 7 (11–12) (2013) 900–903.

[22] D. A. Stewart, P. H. Shipway, D. G. McCartney, (1999). *Abrasive wear behaviour of conventional and nanocomposite HVOF–sprayed WC-Co coatings*, Wear 225-229 (2) 789–798.

[23] C. Lupi, A. Dell'Era, M. Pasquali, P. Imperatori, *Composition, morphology, structural aspects and electrochemical properties of Ni–Co alloy coatings*, Surface and Coatings Technology 205 (23–24) (2011) 5394–5399.

[24] L. Wang, Y. Gao, Q. Xue, H. Liu, T. Xu, *Microstructure and tribological properties of electrodeposited Ni–Co alloy deposits*, Applied Surface Science 242 (3–4) (2005) 326–332.

[25] R. Sruthi, G. S. Rampradheep, K. Raja, *A review on natural plant extract as a green inhibitor for steel corrosion resistance*. International Journal of Advanced Science and Technology 29 (3) (2020) 3529–3550.